

# Lipoamide Channel-Binding Sulfonamides Selectively Inhibit Mycobacterial Lipoamide Dehydrogenase

Ruslana Bryk,<sup>†</sup> Nancy Arango,<sup>§</sup> Christina Maksymiuk,<sup>‡</sup> Anand Balakrishnan,<sup>†</sup> Ying-Ta Wu,<sup>‡</sup> Chi-Huey Wong,<sup>‡</sup> Thierry Masquelin,<sup>@</sup> Philip Hipskind,<sup>@</sup> Christopher D. Lima,<sup>#</sup> and Carl Nathan<sup>\*,†,||</sup>

<sup>†</sup>Department of Microbiology and Immunology and <sup>‡</sup>Department of Pharmacology, Weill Cornell Medical College, New York, New York 10065, United States

<sup>#</sup>Howard Hughes Medical Institute, Structural Biology Program, Sloan-Kettering Institute, New York, New York 10065, United States

<sup>§</sup>Structural Biology Program, Sloan-Kettering Institute, New York, New York 10065, United States

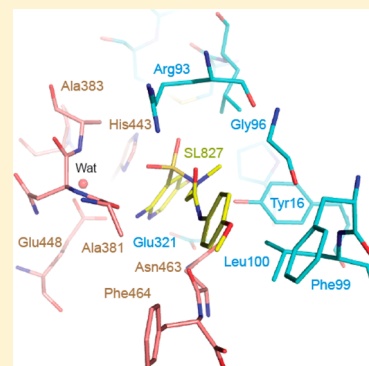
<sup>||</sup>Program in Immunology and Microbial Pathogenesis, Weill Graduate School of Medical Sciences of Cornell University, New York, New York 10065, United States

<sup>‡</sup>Genomics Research Center, Academia Sinica, Taipei 115, Taiwan

<sup>@</sup>Eli Lilly Inc., Indianapolis, Indiana 46285, United States

## S Supporting Information

**ABSTRACT:** Tuberculosis remains a global health emergency that calls for treatment regimens directed at new targets. Here we explored lipoamide dehydrogenase (Lpd), a metabolic and detoxifying enzyme in *Mycobacterium tuberculosis* (Mtb) whose deletion drastically impairs Mtb's ability to establish infection in the mouse. Upon screening more than 1.6 million compounds, we identified *N*-methylpyridine 3-sulfonamides as potent and species-selective inhibitors of Mtb Lpd affording >1000-fold selectivity versus the human homologue. The sulfonamides demonstrated low nanomolar affinity and bound at the lipoamide channel in an Lpd–inhibitor cocrystal. Their selectivity could be attributed, at least partially, to hydrogen bonding of the sulfonamide amide oxygen with the species variant Arg93 in the lipoamide channel. Although potent and selective, the sulfonamides did not enter mycobacteria, as determined by their inability to accumulate in Mtb to effective levels or to produce changes in intracellular metabolites. This work demonstrates that high potency and selectivity can be achieved at the lipoamide-binding site of Mtb Lpd, a site different from the NAD<sup>+</sup>/NADH pocket targeted by previously reported species-selective triazaspirodimeoxybenzoyl inhibitors.



Tuberculosis (TB) remains a global epidemic despite being preventable and treatable. In 2011, an estimated toll of 1.4 million people put TB second in line to only HIV/AIDS as the greatest killer caused by a single infectious agent.<sup>1</sup> New treatment regimens with novel targets are needed to outpace the emergence of drug resistance and deadly associations of TB with HIV and diabetes. One strategy is to target functions that the causative agent, *Mycobacterium tuberculosis*, needs to establish infection and survive host-imposed stress. There are a few known Mtb genes that are nonessential under standard growth conditions *in vitro* but whose loss of function drastically impairs Mtb's ability to survive in the host. Most encode enzymes of central carbon metabolism or detoxification. Among these are lipoamide dehydrogenase, a component of PDH, BCKDH, and peroxynitrite reductase<sup>2–4</sup> in Mtb; phosphoenolpyruvate carboxykinase, PckA, involved in the generation of phosphoenolpyruvate from oxaloacetate during gluconeogenesis;<sup>5</sup> a thiol peroxidase, Tpx;<sup>6</sup> and a probable nitroreductase, Acp,<sup>7</sup> one of the most highly upregulated genes of the *dos* regulon. However, no TB drugs are known to target these enzymes.

Lpd is the E3 component of up to four eukaryotic and prokaryotic central metabolic complexes: PDH, KDH, BCKDH, and the GCS. In Mtb, Lpd serves its classic metabolic function in PDH and BCKDH. However, no KDH or GCS activities have been reported in mycobacteria. Mycobacterial Lpd is uniquely involved in detoxification of reactive oxygen and nitrogen intermediates by serving as a component of NADH-dependent peroxynitrite reductase, along with Dlat, the E2 component of PDH; a thioredoxin-like protein, AhpD; and a peroxiredoxin, AhpC.<sup>3</sup> Mtb lacking Lpd fails to grow with carbohydrates as a sole carbon source *in vitro*, is highly susceptible to RNI, and rapidly dies in mice.<sup>2</sup>

The strict reliance of Mtb's virulence and survival on Lpd *in vivo* drew our attention to Lpd as a target for inhibitors. Bacterial enzymes having human homologues are usually viewed as unattractive targets because of the possible host toxicity of their inhibition. Mycobacterial Lpd is 36% identical

Received: August 8, 2013

Revised: November 13, 2013

Published: November 19, 2013



to the human homologue. The three-dimensional structures of the mycobacterial and human enzyme align closely.<sup>8</sup> However, differences in the substrate-binding sites allow triazaspirodimethoxybenzoyl compounds to act as potent and species-selective mycobacterial Lpd inhibitors.<sup>9</sup> A triazaspirodimethoxybenzoyl inhibitor that was cocrystallized in Mtb Lpd's pocket adjacent to the NAD<sup>+</sup>/NADH-binding site overlapped with the nicotinamide ring-binding site, blocking its coordination with the FAD flavin ring, where it would prevent electron transfer between the cofactors. The compound produced no detectable inhibition of the human homologue, affording at least 100-fold selectivity between the species. However, it had no growth inhibitory effect on whole mycobacteria. This was interpreted as a probable lack of accumulation in the bacterial cells.<sup>9</sup>

To continue the search for mycobacterial Lpd inhibitors, we screened a collection of >1.6 million compounds at the Genomics Research Center at Academia Sinica. Here we report the identification and characterization of a new class of sulfonamides as potent, species-selective inhibitors of Mtb's Lpd. A cocrystal revealed that, in contrast to the triazaspirodimethoxybenzoyls, 2-(2-amino-5-bromo-*N*-methylpyridine-3-sulfonamido)-*N*-(4-methoxyphenyl)acetamide binds at the lipoamide channel of Mtb's Lpd, exploiting a second route to species-selective inhibition.

## ■ EXPERIMENTAL PROCEDURES

**Screening Library.** The compound library at the Genomics Research Center (GRC) of Academia Sinica contained >1.6 million mostly druglike structures (the GRC-2M library), consisting of diversified synthetic compounds (diversity of ~86%), known drugs, named chemicals with a range of biological activities, purified plant and microbial products, and fractionated natural products. The compounds were stored in 384-well and 1536-well formats at −50 °C. For screening, one copy of the library in 100% DMSO was dispensed to 1536-well microtiter plates at a concentration of 1 mM in 50 nL using an online robotic system.

**High-Throughput Screening of Lpd.** We used a modified DTNB reductase assay.<sup>9</sup> Lpd (100 nM) in 100 mM sodium phosphate buffer (pH 7.0) was dispensed in amounts of 4  $\mu$ L/well into 1536-well clear bottom assay plates followed by GRC-2M library compounds. After 1 h at room temperature (RT), 4  $\mu$ L of reaction mixture containing the substrate lipoamide (2 mM), NADH (200  $\mu$ M), and EDTA (4 mM) was added per well, resulting in concentrations of 50 nM Lpd, 1 mM lipoamide, and 6.25  $\mu$ M library compounds. After 5 min, the detection reagent DTNB, prepared as a 375  $\mu$ M stock in 100 mM sodium phosphate buffer (pH 7.0), was added in amounts of 2  $\mu$ L/well, resulting in a final concentration of 75  $\mu$ M. TNB production was recorded by absorbance at 405 nm. *Z'* values for the screen were >0.51. Signal normalization using the median of each plate was applied during data analysis. The histogram of the accumulating number against activity signal was plotted to decide the cutoff.

**Proteins.** Recombinant Mtb proteins were expressed with (His-AceE) or without fusion tags (Lpd and DlaT) in *Escherichia coli* and purified as described previously.<sup>3,4,10</sup> Native bovine liver thioredoxin reductase was purified from calf liver as reported previously.<sup>11</sup> Purified recombinant human Lpd was a generous gift from M. Patel (University at Buffalo, the State University of New York, Buffalo, NY).

**Enzyme Assays.** IC<sub>50</sub> values were determined with serial dilutions (from 100 to 0.1  $\mu$ M) of inhibitors by a

spectrophotometric assay with DTNB, lipoamide, and NADH<sup>9</sup> or a PDH assay<sup>4</sup> as described previously. Human Lpd was assayed with 10  $\mu$ M lipoamide by the same DTNB assay. Bovine thioredoxin reductase was assayed with 100  $\mu$ M NADPH and 75  $\mu$ M DTNB. NADH was detected by absorbance at 340 nm or fluorescence using a Molecular Devices SpectraMax M5 plate reader. Curves were fit using IGOR Pro (WaveMetrics, Portland, OR) version 4.06A Carbon with the Hill equation:  $Y = Y_{\max}/[1 + (IC_{50}/[I])^n]$ , where *n* is the Hill coefficient. Kinetic parameters were determined by the NADH-lipoamide fluorimetric assay at variable substrate (0.2–5 mM lipoamide and 3.33–100  $\mu$ M NADH) and increasing inhibitor (0, 0.01, 0.03, 0.1, 0.3, 0.6, and 0.9  $\mu$ M) concentrations in the presence of 20  $\mu$ M NAD<sup>+</sup> to relieve inhibition by NADH and obtain hyperbolic plots.<sup>10</sup> *K*<sub>m</sub> and *V*<sub>max</sub> values were determined by fitting the data to the hyperbolic function  $V = (V_{\max}X)/(K_m + X)$ . *K*<sub>i</sub> values were determined from nonlinear regression analysis in Prism by fitting data to the equation for noncompetitive inhibition  $V = V_{\max}/(1 + [I]/K_i) \times X/(K_m + X)$  (NADH substrate) or competitive inhibition  $V = (V_{\max}X)/[K_m(1 + [I]/K_i) + X]$  (lipoamide substrate).

**MIC Assay.** MIC values for mycobacteria were determined in 96-well plates in 200  $\mu$ L of Middlebrook 7H9 medium (pH 6.6) with 0.2% glycerol, 0.05% Tween 80, and 10% ADN (5% BSA, 2% dextrose, and 0.85% NaCl). The starting bacterial inoculum was 0.1 or 0.01 (OD<sub>580</sub>). Inhibitors were tested at 2-fold serial dilutions from 100 to 0.1  $\mu$ M. MICs were defined as compound concentrations that inhibited bacterial growth >90%.

**Crystallization and Structure Determination.** Mtb Lpd expression and purification for crystallographic analysis were performed as reported previously.<sup>8,9</sup> Lpd (200  $\mu$ M), inhibitor SL827 (300  $\mu$ M), and 600  $\mu$ M NADH were mixed and incubated on ice for 10 min prior to crystallization at 18 °C by hanging drop vapor diffusion against a well solution containing 100 mM Tris (pH 8.5), 50 mM NaCl, and 19% (w/v) PEG 10000. Crystals were cryo-protected by addition of 25% glycerol and flash-cooled in liquid nitrogen. A single crystal was diffracted, and data were collected at NE-CAT beamline 24-IDC at 0.9795 Å to obtain a data set at 2.6 Å resolution. The structure of Lpd bound to SL827 was determined by molecular replacement using programs contained within CCP4<sup>12</sup> and our previously determined structure of Lpd.<sup>8</sup> The crystal lattice included two dimers in the asymmetric unit and a model comprising Lpd amino acids 1–464 and an additional N-terminal Ser residue that remained from the cleavage tag (Gly-Ser). This model was refined using Phenix<sup>13</sup> after manual rebuilding in O<sup>14</sup> and Coot;<sup>15</sup> 459 water molecules and SL827 were added to the model and refined to *R* and *R*<sub>free</sub> values of 0.169 and 0.222, respectively, at 2.4 Å (Table 1). The model has excellent geometry with 91.7 and 8.3% of residues in favored and allowed regions of the Ramachandran plot, respectively, as calculated by Procheck<sup>16</sup> with MolProbity scores for all atom contacts and protein geometry in the 100th and 99th percentiles, respectively.<sup>17</sup> Atomic coordinates and structure factors have been deposited in the Protein Data Bank as entry 4MS2.

**Determination of the Intracellular Accumulation of Sulfonamide by Metabolic Profiling.** Wild-type H37Rv Mtb was grown in 7H9 Middlebrook medium supplemented with 0.2% glycerol, 0.2% dextrose, 0.5% BSA, 0.085% NaCl, and 0.05% Tween 80 to an OD<sub>580</sub> of 1.0. One milliliter of culture

**Table 1. Data Collection and Refinement Statistics of the Lpd–Compound SL827 Complex**

Data Collection <sup>a,b</sup>	
space group	P2 <sub>1</sub>
cell dimensions	
<i>a</i> , <i>b</i> , <i>c</i> (Å)	82.52, 111.95, 98.03
$\alpha$ , $\beta$ , $\gamma$ (deg)	90, 94.43, 90
resolution (Å)	40–2.4 (2.44–2.40)
total no. of reflections	202954
no. of unique reflections	67889 (3369)
Wilson <i>B</i>	30.0
<i>R</i> <sub>merge</sub>	0.097 (0.475)
<i>R</i> <sub>pim</sub>	0.066 (0.318)
<i>I</i> / $\sigma$ <i>I</i>	15.5 (3.6)
completeness (%)	96.1 (95.7)
redundancy	3.0 (3.0)
Refinement <sup>b</sup>	
resolution (Å)	40–2.4 (2.43–2.4)
no. of reflections	66805/2600
<i>R</i> <sub>work</sub> <i>R</i> <sub>free</sub>	16.9 (20.7), 22.2 (28.6)
no. of atoms	
protein	13900
FAD	212
SL827	100
water	459
average <i>B</i> factor	
protein (protomer A/B/C/D)	37.2/39.4/37.9/41.2
FAD (protomer A/B/C/D)	30.6/35.2/30.7/33.3
SL827 (protomer A/B/C/D)	36.0/44.7/40.1/41.1
water	38.5
root-mean-square deviation	
bond lengths (Å)	0.004
bond angles (deg)	0.880
MolProbity score	
all atom contacts	100th percentile
protein geometry	99th percentile

<sup>a</sup>One crystal. <sup>b</sup>Data for the Highest-resolution shell given in parentheses.

was filtered through a hydrophilic PVDF membrane (0.22  $\mu$ m, Millipore GVWP02500). Both blank (no Mtb) and Mtb-bearing filters were placed atop 7H10 agar plates (with 0.2% glycerol, 0.2% dextrose, and 0.085% NaCl) without detergent. Plates were incubated at 37 °C in 5% CO<sub>2</sub>. After 5 days, filters were transferred to 7H10 agar plates containing either 75  $\mu$ M compound or an equal volume of 100% DMSO (vehicle control) for 24 h. Filters were flipped into a 1 mL ice-cold 40:40:20 methanol/acetonitrile/water solution. Mtb was scraped off filters and lysed via bead beating three times. Blank filters (on agar with and without compound) were processed as reported previously.<sup>2,18,19</sup> Small molecule extracts were mixed in a 1:1 ratio with an acetonitrile and 0.2% formic acid solvent for MS analysis. To determine compound intracellular uptake, a standard curve was generated by spiking mycobacterial small molecule extract with known concentrations of compound to correct for ion suppressive effects of the lysate. To assess metabolite abundance, protein was measured using a Pierce BCA kit, and ion counts of specified metabolites were normalized to protein concentration.

## RESULTS

**High-Throughput Screening for Lpd Inhibitors.** After screening 1622277 compounds from the GRC-2M library, we selected 11458 (~0.7% hit rate) for further evaluation on the basis of achieving  $\geq 25\%$  inhibition. These primary hits included some natural products and known drugs that were previously shown to inhibit Lpd.<sup>9</sup> The primary hits were retested in an eight-point concentration–response assay ( $Z' = 0.74$ ). Compounds with IC<sub>50</sub> values of  $< 5 \mu$ M were selected (283 compounds). A small fraction of the hits (5%) were quinones. Because Mtb's Lpd can reduce quinones more efficiently than lipoamide,<sup>10</sup> these were considered false positives and were excluded from further studies. Structure similarity analysis showed that many of the remaining inhibitors clustered into four major scaffolds: pyrimido[5,4-*e*][1,2,4]triazine-5,7-diones, pyrrolo[2,3-*b*]quinoxaline, 1*H*-quinolin-2-ol, and imidazol-4-yl-sulfonyl piperidine (including the *N*-methylpyridine 3-sulfonamides) (Figure 1A).

The most potent inhibitors were triazinediones. Six of these were resupplied from an independent source, and all six inhibited mLpd with IC<sub>50</sub> values in the range of 1–2  $\mu$ M. However, they also inhibited hLpd with comparable potency (IC<sub>50</sub> values of 3–5  $\mu$ M) (Figure 1B). When Lpd was tested for inhibition as a part of the PDH complex along with E1 (AceE) and E2 (DlaT) components, the potency declined by 100–200-fold, suggesting that Lpd in the PDH complex may not be accessible to triazinediones. Likewise, the compounds lost their ability to inhibit mammalian Lpd when they were tested against the bovine PDH complex. Finally, all triazinediones tested were toxic to monkey kidney Vero cells as determined by the MTS assay, with IC<sub>50</sub> values similar to those against isolated mLpd.

Next, we explored the quinoxaline scaffold. Although these compounds produced very little toxicity when they were tested from the library, four structurally related quinoxalines from an independent supplier achieved only 50% inhibition of mycobacterial or human Lpd at or above 100  $\mu$ M, and there was little increase in potency upon storage in DMSO at RT for 10 days (Figure 1C). MS analysis of the compound stocks did not reveal any differences between the inactive and active quinoxalines, suggesting that structural rearrangements affected their function.

Finally, we reordered four sulfonamide inhibitors that belonged to the scaffold, which was most highly over-represented among the hits (36%). All four compounds potentially inhibited mLpd in isolation with *K<sub>i</sub>* values in low nanomolar range and with comparable or slightly less potency against Lpd in the PDH complex (Table 2). Strikingly, at the highest concentration tested (100  $\mu$ M), they did not inhibit hLpd, thus affording at least 400-fold and in some cases >2700-fold species selectivity (Figure 2A and Table 2). Kinetic analysis revealed that the compounds were noncompetitive inhibitors with respect to the NADH substrate but competitive against the lipoamide substrate (Figure 2B,C). This mode of inhibition differed from that of the triazaspirodimethoxybenzoyl Lpd inhibitor that bound at the NAD<sup>+</sup>/NADH site.<sup>9</sup> This suggested that the sulfonamides bind at a different site than the triazaspirodimethoxybenzoyls. To investigate this, we sought to cocrystallize the sulfonamide inhibitor SL827 with Mtb Lpd.

**Structure of the Lpd–Sulfonamide Cocrystal.** The Lpd protein component of the structure resembles that previously determined for Mtb Lpd in the absence of SL827,<sup>8</sup> and while 600  $\mu$ M NADH was present in the crystallization and

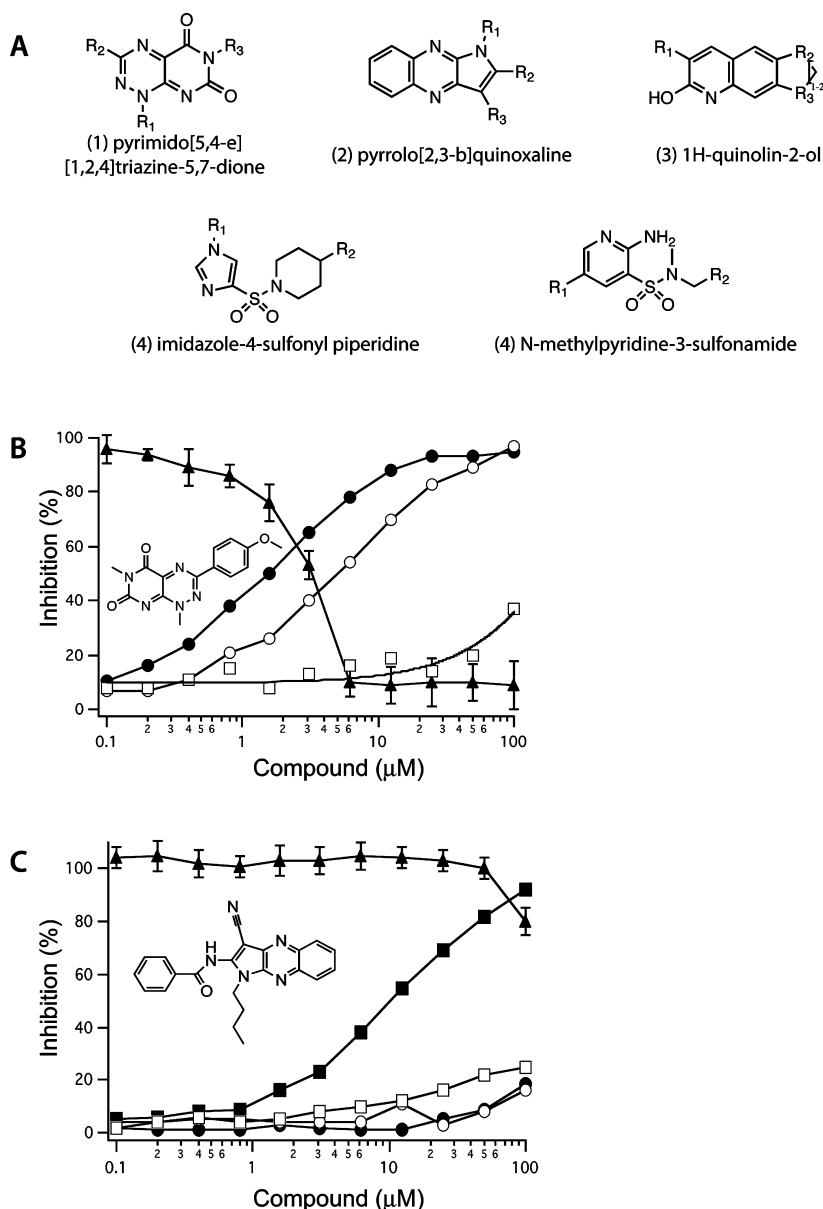


**Figure 1.** Identification of major scaffolds of Mtb Lpd inhibitors (A) and characterization of triazinediones (B) and quinoxaline (C) compounds as Lpd inhibitors. Pure recombinant mLpd (●), hLpd (○), or the mycobacterial PDH complex (□) was tested against the hit compounds (structures shown in the inset) from freshly prepared stocks or after incubation of compound stocks in DMSO at RT (■) for 10 days. The toxicity of compounds (▲) was assessed against the monkey kidney Vero cell line by the MTS assay.

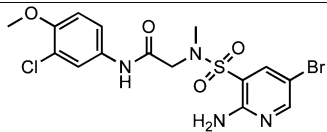
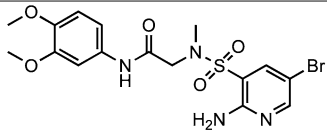
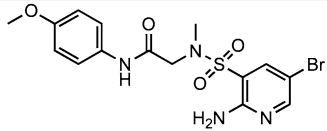
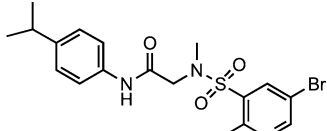
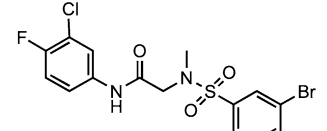
cryopreservation solutions, no NADH was observed in the predicted NADH-binding sites. SL827 occupies a deep pocket adjacent to each of the four active sites (Figure 3A), and each molecule of SL827 adopts a similar configuration up to the paramethoxyaniline ring that differs by a slight rotation due to differences in adjacent lattice contacts, presumably due to the alternative configuration of Phe99 (Figure 3B,C). The deep pocket occupied by SL827 is the presumed binding site for lipoamide and is proximal to the active site cysteine residues (Cys41 and Cys46), which adopt an oxidized, disulfide-bonded configuration (Figure 3A).

SL827 appears in an extended conformation that spans 17 Å from the bromine atom to the methoxy group. Interactions between SL827 and the two Lpd protomers bury approximately 825 Å<sup>2</sup> of total surface area in each of the four binding sites. The bromine atom is <4 Å (Figure 3A) from side chain atoms

of Pro13, His443, and Glu321 (Figure 3A) and 4.2 or 4.4 Å from side chain atoms of Leu42 or Cys41, respectively. The aminopyridine ring is within van der Waals distance of the side chain atoms of Glu321, Tyr16, Asn463, and His443. A direct hydrogen bond is observed between its amine nitrogen and the backbone carbonyl oxygen atom of Ala381 in addition to a water-mediated hydrogen bond between the amine nitrogen of the aminopyridine ring and the side chain carboxylate of Glu448 and the backbone amide of Ala383. The sulfonamide group does not make any close contacts with the Lpd structure, with the exception of a potential hydrogen bond interaction between the sulfonamide oxygen and the backbone amide of Ala383. Hydrogen bonds are observed between the amido oxygen of SL827 and the Arg93 guanidinium and the amido nitrogen of SL827 and the backbone carbonyl oxygen of Asn463, suggesting that this region of the SL827 structure is



Table 2. Sulfonamide Inhibitors of Mycobacterial Lpd

ID	Structure	K <sub>i</sub> (Lpd), nM	K <sub>i</sub> (PDH), nM	SI <sup>a</sup>
SL932		37±5	78±6	>2700
SL809		93±12	155±12	>1075
SL827		140±9	155±14	>714
SL917		233±15	289±9	>429
SL418		143±12	333±28	1300

<sup>a</sup>Because of the solubility limit of the compounds, the highest concentration tested was 100  $\mu$ M. No inhibition of hLpd by SL932, SL809, SL827, or SL917 was observed at 100  $\mu$ M, and the SI values were calculated using 100  $\mu$ M as a substitute K<sub>i</sub> value for hLpd. The resulting SI therefore reflects the lower limit of the SI value and in fact will be much greater, which is indicated by the greater than symbol.

important for imparting interactions to specific groups within SL827 (see below). Although proximal to side chain atoms from Phe99, Leu100, and Phe464, the paramethoxyaniline ring is not well coordinated by the Lpd structure, perhaps consistent with the two conformations and weaker electron density observed for this segment of SL827 in the crystal structure (Figure 3B–D).

**SL827 Contacts with R93 Are Critical for Its Inhibitory Activity.** A solution of the Mtb Lpd crystal structure<sup>8</sup> revealed a prominent difference between the mammalian and mycobacterial Lpd structures in the architecture of the residues lining the lipoamide-binding channel. Arg93, which is conserved among mycobacterial Lpds but not eukaryotic Lpd family members, was observed in two different conformations in each monomer of the dimer, with the side chain pointing away from (“open” state) or into (“closed” state) the active site channel. Therefore, we explored if contacts of SL827 with Arg93 contributed to its species selectivity by testing the ability of SL827 to inhibit the R93A mutant of mycobacterial Lpd. The  $V_{\max}$  of the R93A mutant is 40-fold lower than that of the wild type when lipoamide is present in solution, but the mutant enzyme retains the ability to accommodate lipoamide when it is presented as being attached to the E2 component of PDH.

Thus, we assessed the inhibition of Lpd by SL827 in the PDH complex containing AceE (E1), DlaT (E2), and either wild-type (WT) Lpd or R93A Lpd. As predicted, SL827 was unable to efficiently inhibit R93A Lpd even at the highest concentration tested, 100  $\mu$ M (Figure 4). The K<sub>i</sub> for SL827 increased >600-fold when R93A Lpd was substituted for WT Lpd in the PDH complex from 0.15 to 100  $\mu$ M, suggesting that the contacts made between the SL827 and Arg93 are critical for correct positioning of the inhibitor in the lipoamide channel.

**Structure–Activity Studies of Sulfonamide Inhibitors.** The GRC-2M library contained 299 structurally related heteroaryl sulfonamide compounds. Of those, 127 imidazol-4-yl-sulfonyl piperidines and 14 *N*-methylpyridine-3-sulfonamides scored as primary hits. After the reconfirmation assay, 61 imidazol-4-yl-sulfonyl piperidines and six *N*-methylpyridine-3-sulfonamides produced IC<sub>50</sub> values of <5  $\mu$ M. Imidazol-4-yl-sulfonyl piperidines were excluded from further studies because they did not inhibit PDH activity as potently as *N*-methylpyridine-3-sulfonamides, suggesting that they cannot compete efficiently with the lipoamide substrate when it is presented in its natural form on the DlaT protein. From the cocrystal structure, we inferred that the numerous bonds between the 2-amino-5-bromopyridine ring of *N*-methylpyr-

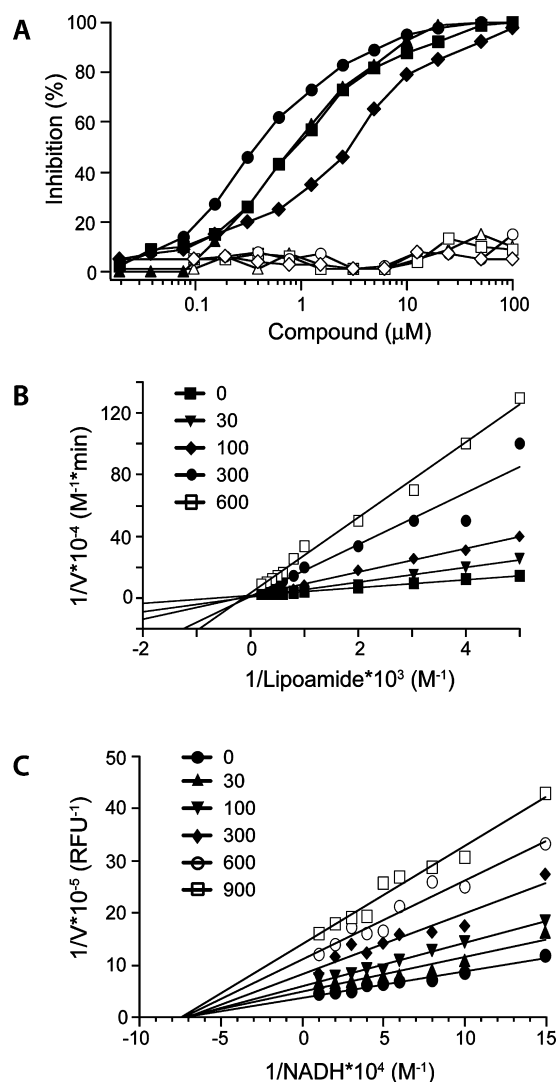


**Figure 2.** Characterization of sulfonamide Lpd inhibitors. (A) Sulfonamides SL932 (circles), SL809 (triangles), SL827 (squares), and SL917 (diamonds) potentially inhibit pure recombinant mLpd (filled symbols) but not hLpd (empty symbols). Sulfonamide SL827 is competitive with lipoamide (B) substrate and noncompetitive with NADH (C) substrate. The DTNB assay used variable lipoamide (in panel B, 0.1–5 mM), and the NADH-lipoamide fluorimetric assay used variable NADH (in panel C, 3.33–100  $\mu\text{M}$ ). Both assays were run with variable SL827 concentrations as shown. Data were fit in Prism to a nonlinear regression function for competitive or noncompetitive inhibition. Double-reciprocal Lineweaver–Burk plots are shown.

idine-3-sulfonamides and Lpd's side chains and the sulfonamide's perfect alignment within the lipoamide channel, allowing for hydrogen bonding of the amide oxygen with Arg93, account for the greater affinity of *N*-methylpyridine-3-sulfonamides for Mtb Lpd and allow the compounds to efficiently compete with lipoamide in its natural milieu. In contrast, the greater length of imidazol-4-yl-sulfonyl piperidines may not allow for hydrogen bonding between the amide oxygen and Arg93, and the smaller imidazole ring may not maintain enough contacts necessary to compete with the lipoamide substrate. To further study the structure–activity relationship (SAR) of the *N*-methylpyridine-3-sulfonamides, we ordered 11 commercially available structurally related compounds. Substitutions at the meta and para positions of the aniline ring did not affect the potency of

sulfonamides, consistent with the lack of interactions to coordinate the ring as observed in the crystal structure. Compounds with more than one substitution of the aniline ring had consistently lower  $\text{IC}_{50}$  values, suggesting that additional side chains may help stabilize and coordinate the ring (Table 2 and Table 1 of the Supporting Information). In contrast, perturbation of the Asn463 backbone carbonyl H-bonding with the NH group of  $-\text{CONH}-$  by *N*-alkylation led to a 100-fold loss of potency (E114-0951 and E144-0828 in Table 1 of the Supporting Information). In addition, increasing the linker length by one carbon led to an even greater loss of potency (K906-3123 in Table 1 of the Supporting Information), presumably because of the loss of hydrogen bonding with Arg93 via the amide oxygen. Thus, the amide's hydrogen bonding and its alignment within the lipoamide channel are crucial for the activity of the *N*-methylpyridine-3-sulfonamides.

To further expand the SAR, we tested 380 related compounds from the collection of Eli Lilly and Co. through the auspices of the Lilly TB Drug Discovery Initiative. The most potent compound, SL418 (Table 2) ( $K_i = 143 \text{ nM}$ ), was closely related to SL827, differing only in the two side chain substitutions on the aniline ring in place of the methoxy of SL827 (Table 2). Like SL827, SL418 did not inhibit human Lpd and produced a species selectivity index of 1300.

**Uptake of Sulfonamide by and Action within Intact Mycobacteria.** The most active sulfonamide inhibitors, SL827, SL932, SL809, SL917, and SL418, were tested for their effect on intact mycobacteria using a conventional MIC assay with a highest compound concentration of 100  $\mu\text{M}$ . No growth inhibition of *Mycobacterium bovis* BCG or *M. tuberculosis*  $\Delta\text{panCD}\Delta\text{lysA}$  was observed after 7 days in culture in the presence of inhibitors except at 100  $\mu\text{M}$ . All compounds potentially inhibited Lpd activity in mycobacterial lysates as measured by the PDH assay. Nor did we see any growth inhibition of *M. bovis* BCG when we tested the less potent sulfonamides listed in Table 1 of the Supporting Information. The inability of sulfonamides to phenocopy the growth inhibitory effect of *lpd* deletion<sup>2</sup> suggested that the compounds did not accumulate within mycobacteria to effective levels.

To test this, we used a metabolomic profiling platform<sup>18–20</sup> to determine compound uptake and its effect on Mtb's intracellular metabolites. *M. tuberculosis* H37Rv was grown on filters as reported previously.<sup>18,19</sup> Filters with or without Mtb were transferred to agar plates containing 75  $\mu\text{M}$  SL827 for 24 h and harvested in aqueous acetonitrile and methanol for liquid chromatography–mass spectrometry analysis. No Mtb-associated SL827 was observed on filters with mycobacteria compared to empty filter controls (Figure 5), suggesting that SL827 did not enter, was pumped out, or was rapidly converted to another product by adduction or metabolism.

To test whether SL827 was effectively inhibiting Lpd, despite being inapparent in the lysate, we analyzed its impact on Mtb metabolites. Deletion of *lpd* from Mtb results in the accumulation of reaction substrates (pyruvate,  $\alpha$ -ketoisovalerate,  $\alpha$ -ketoisocaproate, and  $\alpha$ -ketomethylvalerate) of Lpd as well as their derivatives and upstream metabolites (alanine, valine, leucine, and isoleucine). Pyruvate and branched chain ketoacids accumulate to levels 100–1000-fold above that of the WT.<sup>2</sup> However, exposure of Mtb to 75  $\mu\text{M}$  SL827 (Figure 5B) produced no changes in the levels of alanine, valine, or leucine, confirming that extracellular application of the compound did not extensively inhibit intracellular Lpd.

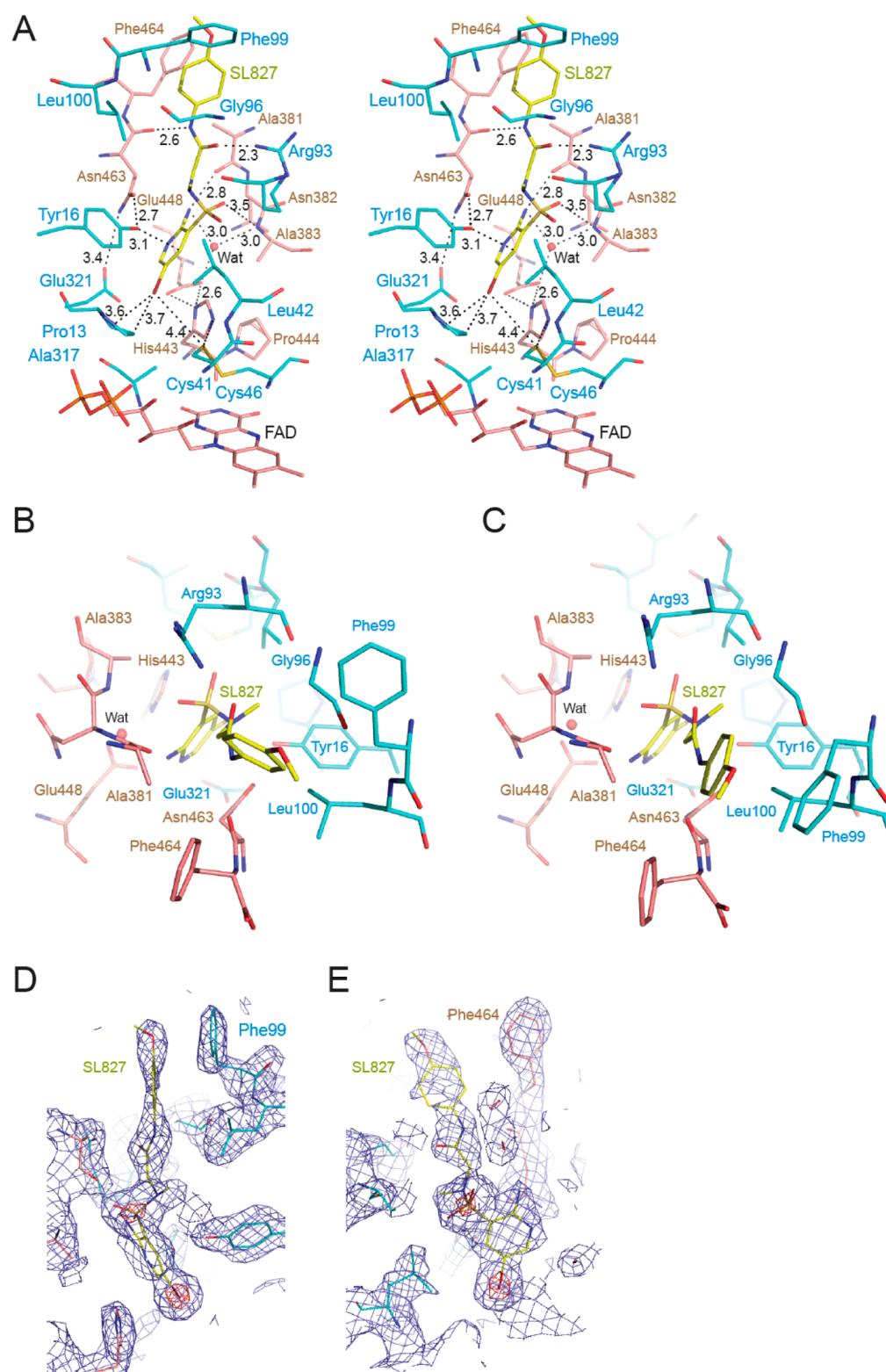


**Figure 3.** Complex between Mtb Lpd and SL827. (A) Stereoview of the Lpd dimer interface bound to SL827. SL827 is colored in CPK with carbon atoms colored yellow. Protomers of Lpd are colored in CPK, one with carbons colored cyan and the other with carbons colored salmon. Amino acid side chains are labeled and colored corresponding to carbon color codes. Potential hydrogen bonds and van der Waals contacts are indicated by black dashed lines with distances in angstroms. The SL827 methoxy group points toward solvent, and the bromine atom points toward the catalytic cysteine residues (Cys41 and Cys46). The FAD cofactor is labeled and located at the bottom of this view. (B) View of SL827 and select amino acids from the dimer interface illustrated in panel A with similar color coding and selected amino acids labeled. (C) Alternative conformation of Phe99 and SL827 as observed in two of the four protomers in the crystal structure. (D and E) Nearly orthogonal views of SL827 as observed in panel A covered by electron density contoured at 1.2 $\sigma$  (blue) and 6.0 $\sigma$  (red), with the latter indicating positions of sulfur and bromine atoms, respectively. Select residues and SL827 are labeled. Electron density was obtained from a simulated annealing omit map ( $2F_o - F_c$ ) calculated using CNS.<sup>29</sup> Figures were generated using PyMol.<sup>30</sup>

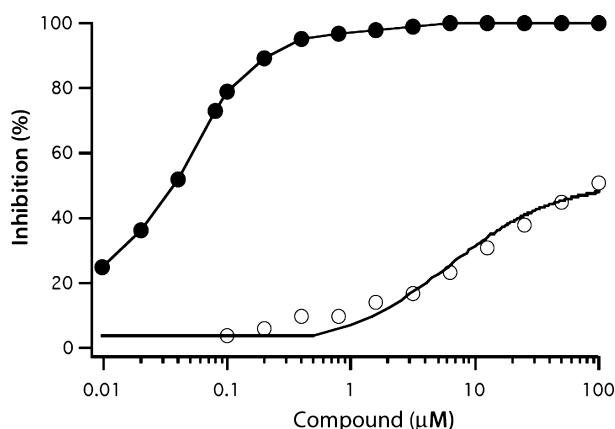


**Figure 4.** SL827 inhibits Mtb PDH composed of AceE, DlaT, and WT Lpd (●) but not the complex composed of AceE, DlaT, and the R93A Lpd mutant (○).

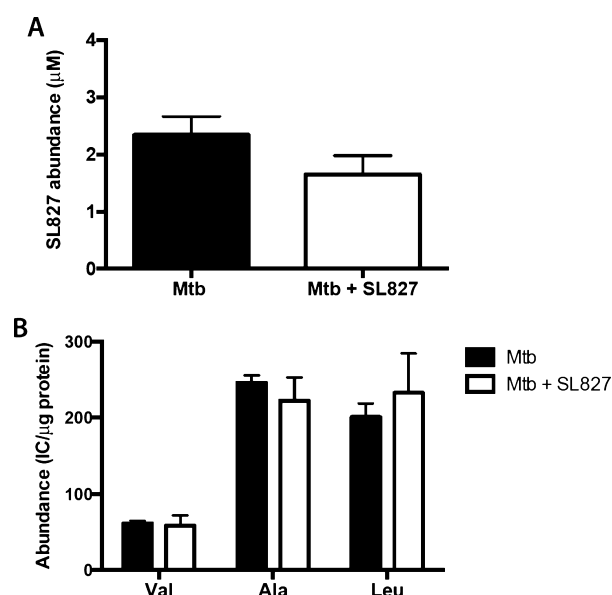


**Figure 5.** SL827 does not accumulate in Mtb. Levels of SL827 accumulation (A) and intracellular metabolites (B) were determined in small molecule extracts from Mtb treated with vehicle control (black) or SL827 (white).

The absence of detectable intracellular SL827 within Mtb and the lack of evidence for its impact suggested that the compound either did not penetrate the cells or was efficiently pumped out, as described for several chemical scaffolds.<sup>21,22</sup> Accordingly, we tested Mtb's sulfonamide susceptibility in the presence of efflux pump inhibitors verapamil and reserpine at concentrations (50 and 25  $\mu$ M, respectively) that produced no growth inhibitory effect on Mtb on their own. All Lpd inhibitory sulfonamides tested on Mtb  $\Delta$ panCD $\Delta$ lysA produced no growth inhibition except at the highest concentration tested, 100  $\mu$ M, and the results were the same in the presence or absence of verapamil and reserpine.

## DISCUSSION

Phenotypic screens are usually preferred in antibiotic discovery because they weed out compounds that fail to accumulate in the pathogen. However, phenotypic screens present their own challenges, among them the fact that the *in vitro* screening conditions may differ critically from the conditions in the

host,<sup>23</sup> and it may be difficult or impossible to identify the inhibitors' molecular targets. Target-based screening is a reasonable complementary approach for molecular targets of particular interest, even if the inhibitors provide only a starting point.

Lpd is one of the few enzymes identified in Mtb that are readily susceptible to inhibition with small chemical compounds and in whose absence the pathogen becomes avirulent in the mouse. We have previously shown that it is possible to inhibit mycobacterial Lpd without inhibiting human Lpd by exploiting amino acid differences in the NAD<sup>+</sup>/NADH-binding site.<sup>8,9</sup> Moreover, evidence that effective anti-infectives often have more than one target is mounting, as recently demonstrated for the established tuberculosis drug *p*-amino-salicylic acid<sup>20</sup> and the experimental tuberculosis pro-drug PA824, a nitroimidazo-oxazine with multiple mechanisms of action, including inhibition of cell wall biosynthesis and respiration<sup>24</sup> and donation of an NO-like species<sup>25</sup> that is likely to have multiple targets of its own.<sup>26</sup> Lpd offers the opportunity to inhibit a single molecular target that participates in three known enzymatic complexes in Mtb that have roles in metabolism and detoxification.<sup>2,3</sup>

Herein, we have identified a second site in mycobacterial Lpd at which a potent inhibitor binds with more than 1000-fold species selectivity. Selectivity could be attributed, at least partially, to the interaction of the sulfonamide backbone and/or side chains with Arg93 within the lipoamide channel. The R93A Mtb Lpd mutant protein was inhibited by the sulfonamide much less efficiently than the wild type, suggesting that those contacts are necessary to position the compound within the channel to achieve inhibition. Human Lpd encodes Leu at the same position.

However, Mtb appeared to be impermeable to the sulfonamide Lpd inhibitors. Not only did exposure of intact mycobacteria to inhibitor produce no change in Lpd substrate levels or bacterial growth rate, but we could not detect the inhibitor itself within the cells. This was unexpected, because sulfonamides were among the first drugs used to treat tuberculosis. It has been assumed that sulfamethoxazole and sulfanilamide, sulfonamides with little or no growth inhibitory effect on Mtb, do not accumulate within the bacteria. However, it was recently demonstrated that these compounds do enter Mtb readily but undergo chemical modification to inactive forms.<sup>20</sup> Even so, the index sulfonamides were detectable, in contrast to the Lpd inhibitor studied here. However, we cannot exclude the possibility that compound SL827 may have been taken up and inactivated so rapidly that none was detected.

Domagk's discovery of the azodye Prontosil pioneered the studies on sulfonamides almost a century ago. Prontosil proved to be a prodrug that was metabolized to an active sulfonamide. Later studies suggested that sulfonamides enter bacteria via passive diffusion in a manner governed in part by the  $pK_a$  of the compound and the extracellular–intracellular pH gradient.<sup>27,28</sup> All sulfonamide antibiotics currently in use, such as sulfisoxazole, sulfadiazine, sulfacetamide, sulfamethoxazole, and sulfadoxine, have  $pK_a$  values ranging from 5.0 to 6.5. In contrast, the most basic of the predicted  $pK_a$  values of the sulfonamide compounds reported here range from 11.77 to 13.00, but because of their amphoteric nature, they are predicted to exist mostly as noncharged molecules at physiological pH and thus would be expected to enter by passive diffusion. Therefore, it remains unclear why we did not detect SL827 inside Mtb. It is possible that other



physicochemical properties of the Lpd inhibitory sulfonamides affect their uptake, such as polar surface area and lipophilicity. We are hopeful that a more extensive SAR analysis will identify analogues that preserve nanomolar potency and acquire the ability to accumulate within Mtb.

## ■ ASSOCIATED CONTENT

### ■ Supporting Information

Additional structures and their IC<sub>50</sub> values and levels of inhibition. This material is available free of charge via the Internet at <http://pubs.acs.org>.

### ■ Accession Codes

The atomic coordinates and structure factors have been deposited in the Protein Data Bank as entry 4M52.

## ■ AUTHOR INFORMATION

### ■ Corresponding Author

\*E-mail: [cnathan@med.cornell.edu](mailto:cnathan@med.cornell.edu). Telephone: (212) 746-6505. Fax: (212) 746-8587.

### ■ Funding

This work was supported by National Institutes of Health Grant AI064768, the Abby and Howard P. Milstein Program in Chemical Biology and Translational Medicine, and the Howard Hughes Medical Institute. The collaboration was fostered by the Lilly TB Drug Discovery Initiative. The Department of Microbiology and Immunology is supported by the William Randolph Hearst Foundation. C.D.L. is an investigator of the Howard Hughes Medical Institute.

### ■ Notes

The authors declare no competing financial interest.

## ■ ACKNOWLEDGMENTS

We thank Yan Ling for recombinant protein purification, David Warren for chemical synthesis, Madhumitha Nandakumar and Sumit Chakraborty for help with metabolomic profiling and discussion of results, Kristin Burns-Huang for helpful discussions, and Prof. M. Patel (University at Buffalo, the State University of New York) for the generous gift of pure recombinant human Lpd. We thank the MSKCC X-ray core for use of their facility.

## ■ ABBREVIATIONS

Mtb, *M. tuberculosis*; Lpd, lipamide dehydrogenase; hLpd, human lipamide dehydrogenase; mLpd, mycobacterial lipamide dehydrogenase; TB, tuberculosis; HIV, human immunodeficiency virus; PDH, pyruvate dehydrogenase complex; PNR/P, peroxynitrite reductase/peroxidase; KDH,  $\alpha$ -ketoglutarate dehydrogenase complex; BCKDH, branched chain ketoacid dehydrogenase complex; GCS, glycine cleavage system; DlaT, dihydrolipamide acyltransferase; AhpD, alkyl hydroperoxide reductase subunit D; RNI, reactive nitrogen intermediates; DTNB, 5,5'-dithiobis(2-nitrobenzoic acid); OD, optical density; MIC, minimal inhibitory concentration that inhibits bacterial growth by >90%; MTS, 3-(4,5-dimethylthiazol-2-yl)-5-(3-carboxymethoxyphenyl)-2-(4-sulfophenyl)-2H-tetrazolium; SI, selectivity index.

## ■ REFERENCES

- (1) World Health Organization (2012) Global tuberculosis report 2012, World Health Organization Press, Geneva.
- (2) Venugopal, A., Bryk, R., Shi, S., Rhee, K., Rath, P., Schnappinger, D., Ehrh, S., and Nathan, C. (2011) Virulence of *Mycobacterium*

*tuberculosis* depends on lipamide dehydrogenase, a member of three multienzyme complexes. *Cell Host Microbe* 9, 21–31.

- (3) Bryk, R., Lima, C. D., Erdjument-Bromage, H., Tempst, P., and Nathan, C. (2002) Metabolic enzymes of mycobacteria linked to antioxidant defense by a thioredoxin-like protein. *Science* 295, 1073–1077.

- (4) Tian, J., Bryk, R., Shi, S., Erdjument-Bromage, H., Tempst, P., and Nathan, C. (2005) *Mycobacterium tuberculosis* appears to lack  $\alpha$ -ketoglutarate dehydrogenase and encodes pyruvate dehydrogenase in widely separated genes. *Mol. Microbiol.* 57, 859–868.

- (5) Marrero, J., Rhee, K. Y., Schnappinger, D., Pethe, K., and Ehrh, S. (2010) Gluconeogenic carbon flow of tricarboxylic acid cycle intermediates is critical for *Mycobacterium tuberculosis* to establish and maintain infection. *Proc. Natl. Acad. Sci. U.S.A.* 107, 9819–9824.

- (6) Hu, Y., and Coates, A. R. (2009) Acute and persistent *Mycobacterium tuberculosis* infections depend on the thiol peroxidase Tpx. *PLoS One* 4, e5150.

- (7) Hu, Y., and Coates, A. R. (2011) *Mycobacterium tuberculosis* *acg* gene is required for growth and virulence in vivo. *PLoS One* 6, e20958.

- (8) Rajashankar, K. R., Bryk, R., Kniewel, R., Buglino, J. A., Nathan, C. F., and Lima, C. D. (2005) Crystal structure and functional analysis of lipamide dehydrogenase from *Mycobacterium tuberculosis*. *J. Biol. Chem.* 280, 33977–33983.

- (9) Bryk, R., Arango, N., Venugopal, A., Warren, J. D., Park, Y. H., Patel, M. S., Lima, C. D., and Nathan, C. (2010) Triazaspirodimethoxybenzoyls as selective inhibitors of mycobacterial lipamide dehydrogenase. *Biochemistry* 49, 1616–1627.

- (10) Argyrou, A., and Blanchard, J. S. (2001) *Mycobacterium tuberculosis* lipamide dehydrogenase is encoded by Rv0462 and not by the *lpdA* or *lpdB* genes. *Biochemistry* 40, 11353–11363.

- (11) Holmgren, A. (1997) Bovine thioredoxin system. Purification of thioredoxin reductase from calf liver and thymus and studies of its function in disulfide reduction. *J. Biol. Chem.* 272, 4600–4606.

- (12) Collaborative Computational Project Number 4 (1994) The CCP4 suite: Programs for protein crystallography. *Acta Crystallogr. D* 50, 760–763.

- (13) Adams, P. D., Afonine, P. V., Bunkoczi, G., Chen, V. B., Davis, I. W., Echols, N., Headd, J. J., Hung, L. W., Kapral, G. J., Grosse-Kunstleve, R. W., McCoy, A. J., Moriarty, N. W., Oeffner, R., Read, R. J., Richardson, D. C., Richardson, J. S., Terwilliger, T. C., and Zwart, P. H. (2010) PHENIX: A comprehensive Python-based system for macromolecular structure solution. *Acta Crystallogr. D* 66, 213–221.

- (14) Jones, T. A., Zou, J. Y., Cowan, S. W., and Kjeldgaard, M. (1991) Improved methods for building protein models in electron density maps and the location of errors in these models. *Acta Crystallogr. A* 47 (Part 2), 110–119.

- (15) Emsley, P., and Cowtan, K. (2004) Coot: Model-building tools for molecular graphics. *Acta Crystallogr. D* 60, 2126–2132.

- (16) Laskowski, R. A., Moss, D. S., and Thornton, J. M. (1993) Main-chain bond lengths and bond angles in protein structures. *J. Mol. Biol.* 231, 1049–1067.

- (17) Chen, V. B., Arendall, W. B., III, Headd, J. J., Keedy, D. A., Immormino, R. M., Kapral, G. J., Murray, L. W., Richardson, J. S., and Richardson, D. C. (2010) MolProbity: All-atom structure validation for macromolecular crystallography. *Acta Crystallogr. D* 66, 12–21.

- (18) de Carvalho, L. P., Fischer, S. M., Marrero, J., Nathan, C., Ehrh, S., and Rhee, K. Y. (2010) Metabolomics of *Mycobacterium tuberculosis* reveals compartmentalized co-catabolism of carbon substrates. *Chem. Biol.* 17, 1122–1131.

- (19) de Carvalho, L. P., Zhao, H., Dickinson, C. E., Arango, N. M., Lima, C. D., Fischer, S. M., Ouerfelli, O., Nathan, C., and Rhee, K. Y. (2010) Activity-based metabolomic profiling of enzymatic function: Identification of Rv1248c as a mycobacterial 2-hydroxy-3-oxoadipate synthase. *Chem. Biol.* 17, 323–332.

- (20) Chakraborty, S., Gruber, T., Barry, C. E., III, Boshoff, H. I., and Rhee, K. Y. (2013) Para-aminosalicylic acid acts as an alternative substrate of folate metabolism in *Mycobacterium tuberculosis*. *Science* 339, 88–91.

- (21) Balganes, M., Dinesh, N., Sharma, S., Kuruppath, S., Nair, A. V., and Sharma, U. (2012) Efflux pumps of *Mycobacterium tuberculosis* play a significant role in antituberculosis activity of potential drug candidates. *Antimicrob. Agents Chemother.* 56, 2643–2651.
- (22) Rodrigues, L., Vilellas, C., Bailo, R., Viveiros, M., and Ainsa, J. A. (2013) Role of the Mmr efflux pump in drug resistance in *Mycobacterium tuberculosis*. *Antimicrob. Agents Chemother.* 57, 751–757.
- (23) Pethe, K., Sequeira, P. C., Agarwalla, S., Rhee, K., Kuhlen, K., Phong, W. Y., Patel, V., Beer, D., Walker, J. R., Duraiswamy, J., Jiricek, J., Keller, T. H., Chatterjee, A., Tan, M. P., Ujjini, M., Rao, S. P., Camacho, L., Bifani, P., Mak, P. A., Ma, I., Barnes, S. W., Chen, Z., Plouffe, D., Thayalan, P., Ng, S. H., Au, M., Lee, B. H., Tan, B. H., Ravindran, S., Nanjundappa, M., Lin, X., Goh, A., Lakshminarayana, S. B., Shoen, C., Cynamon, M., Kreiswirth, B., Dartois, V., Peters, E. C., Glynn, R., Brenner, S., and Dick, T. (2010) A chemical genetic screen in *Mycobacterium tuberculosis* identifies carbon-source-dependent growth inhibitors devoid of in vivo efficacy. *Nat. Commun.* 1, 57.
- (24) Manjunatha, U., Boshoff, H. I., and Barry, C. E. (2009) The mechanism of action of PA-824: Novel insights from transcriptional profiling. *Commun. Integr. Biol.* 2, 215–218.
- (25) Singh, R., Manjunatha, U., Boshoff, H. I., Ha, Y. H., Niyomrattanakit, P., Ledwidge, R., Dowd, C. S., Lee, I. Y., Kim, P., Zhang, L., Kang, S., Keller, T. H., Jiricek, J., and Barry, C. E., III (2008) PA-824 kills nonreplicating *Mycobacterium tuberculosis* by intracellular NO release. *Science* 322, 1392–1395.
- (26) Nathan, C. (2008) Microbiology. An antibiotic mimics immunity. *Science* 322, 1337–1338.
- (27) Buttner, D., and Buttner, H. (1980) pH dependency in uptake of sulfonamides by bacteria. *Chemotherapy* 26, 153–163.
- (28) Tappe, W., Zarfl, C., Kummer, S., Burauel, P., Vereecken, H., and Groeneweg, J. (2008) Growth-inhibitory effects of sulfonamides at different pH: Dissimilar susceptibility patterns of a soil bacterium and a test bacterium used for antibiotic assays. *Chemosphere* 72, 836–843.
- (29) Brunger, A. T., Adams, P. D., Clore, G. M., DeLano, W. L., Gros, P., Grosse-Kunstleve, R. W., Jiang, J. S., Kuszewski, J., Nilges, M., Pannu, N. S., Read, R. J., Rice, L. M., Simonson, T., and Warren, G. L. (1998) Crystallography & NMR system: A new software suite for macromolecular structure determination. *Acta Crystallogr. D* 54, 905–921.
- (30) DeLano, W. (2002) *The PyMOL molecular graphics system*, DeLano Scientific, San Carlos, CA.